Applied Materials Today 23 (2021) 101013

Contents lists available at ScienceDirect

Applied Materials Today

journal homepage: www.elsevier.com/locate/apmt

3D flow-focusing microfluidic biofabrication: One-chip-fits-all hydrogel fiber architectures

Carlos F. Guimarães[a,b], Luca Gasperini[a,b], Alexandra P. Marques[a,b], Rui L. Reis[a,b,*]

[a] 3B's Research Group – Biomaterials, Biodegradables and Biomimetics, Headquarters of the European Institute of Excellence on Tissue Engineering and Regenerative Medicine, University of Minho, Ave Park, Parque de Ciência e Tecnologia, Zona Industrial da Gandra, Barco, Guimarães 4805-017, Portugal
[b] ICVS/3B's – PT Government Associate Laboratory, Braga/Guimarães, Portugal

ARTICLE INFO

Article history:
Received 20 January 2021
Revised 13 March 2021
Accepted 16 March 2021

Keywords:
Tissue engineering
Hydrogel microfibers
3D biological models
Cancer models
Vascular fibers

ABSTRACT

The microfluidic manipulation of hydrogels is a powerful tool to recapitulate functional biological architectures. A wide range of flow configurations and chip designs have been employed to create microfibers with increasingly complex shapes and compositions requiring individually engineered setups. Distinctly, we demonstrate how one single 3D hydrodynamic flow-focusing chip can be used to obtain a continuous flow of hydrogel precursors, which rearrange themselves based on viscosity and applied pressures. These can crosslink into fibers with a variety of new multi-compartment shapes down to yet-unreported minimal dimensions. To prove the potential of 3D flow-focusing for the biofabrication of complex, multi-compartment structures, we tuned material properties and flow conditions to obtain ribbon-like cancer/basement-membrane/stroma models; core-shell vascular-like structures and networks; and multi-chemistry fibers integrating stem cells, biomaterials, and pro-differentiation hydrophobic molecule depots. This innovative biofabrication method can be valuable for the recreation of a broad range of complex biological architectures and micro-modeling of distinct 3D environments.

1. Introduction

The fabrication of cell-laden hydrogel microfiber structures represents an exciting approach to recapitulate biological tissues' architecture and functionality at the microscale [1]. Initial strategies for the fabrication of such structures were based mostly on spinning ionic-crosslinking hydrogel precursors, such as alginate, in a core-sheath setup, with the crosslinking solution, e.g., $CaCl_2$, being the sheath to the precursor hydrogel core [2,3]. Over the past decade, these approaches evolved towards more complex shapes to approach a variety of biological tissues [4,5]. Cylindrical hydrogel fibers [2] gradually branched into forms as varied as flat [6], core-shell [7–10], hollow [9], janus [11], helical [8,10], as well as combinations thereof such as hollow Janus [11] or helical core-shell [8] fibers. Most of these geometries are dictated by microfluidic chip designs or needle setups arranged to reproduce a specific shape [4]. Despite these advances, previous approaches present two significant caveats, (1) a clear need to devise a particular microfluidic setup to achieve each of these distinct structures and (2) a limited type of geometries obtained with a single setup.

As an alternative to existing systems, we investigated 3D microfluidic flow-focusing (FF) as an innovative approach for spinning hydrogel precursors into novel multi-material, multi-compartment hydrogel constructs. 3D FF consists of having distinct solutions flowing within separate microfluidic channels, which then meet at a junction or pore, generating a 3D-focused stream composed of all flowing solutions. After this junction, the organization of fluids is dictated by pressure and viscosity, and it is frequently employed for droplet generation with continuous/discontinuous phases [12–15]. Distinctly, we report for the first time how 3D FF can be used to obtain a threading flow regimen of hydrogel precursors to fabricate continuous hydrogel fibers with distinct materials, shapes, and compartments, by tuning the viscosity of solutions and manipulating the pressure applied to the inlets (and consequent flow).

We then employ this tool for the biofabrication of cell-laden hydrogel architectures that approach the dimensions, mechanics, and biological complexity of living tissues, from core-shell vascular-like structures and networks to novel cancer/basement membrane/stroma 3D disease models. We further explore the integration of hydrophobic drug depots in stem-cell-laden fibers, where the multi-chemistry composition allows for an all-in-one tissue en-

* Corresponding author at: 3B's Research Group – Biomaterials, Biodegradables and Biomimetics, Headquarters of the European Institute of Excellence on Tissue Engineering and Regenerative Medicine, University of Minho, Ave Park, Parque de Ciência e Tecnologia, Zona Industrial da Gandra, Barco, Guimarães 4805-017, Portugal.
E-mail address: rgreis@i3bs.uminho.pt (R.L. Reis).

https://doi.org/10.1016/j.apmt.2021.101013
2352-9407/

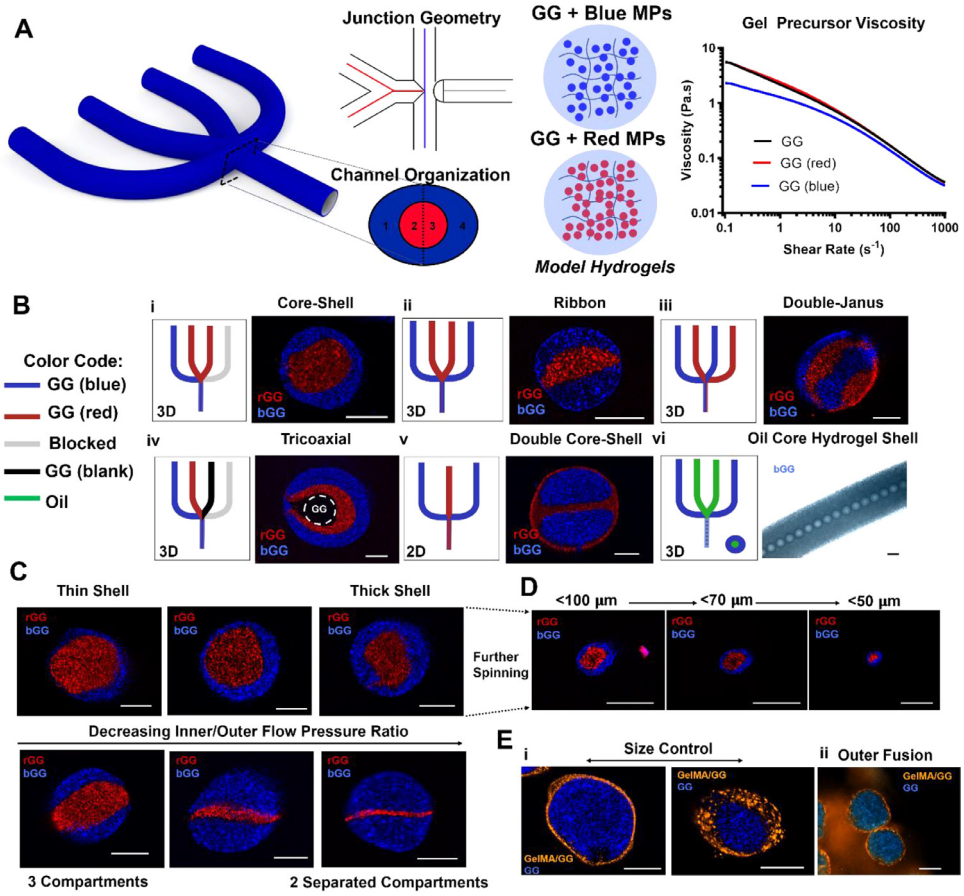

Fig. 1. Flow Focusing Hydrogel Micro Architectures: A | Schematic of 3D Flow-Focusing Chip Channel organization and junction configuration (left). Model Gellan Gum hydrogels encapsulating distinct microparticles and respective viscosity profiles (right). B | Representation of the channel configurations to employ for obtaining different hydrogel fiber shapes: Core-Shell (i), ribbon (ii), double-Janus (iii), tri-coaxial (iv), double Core-Shell (v), and Oil-Core-Hydrogel-Shell (vi). The colors represent the different solutions used, as sketched at the left of each microscope image. bGG - Gellan Gum with blue microparticles, rGG – Gellan Gum with red microparticles. C | Consequence of pressure ratios on the relative size of fiber compartments in the core-shell (top) and ribbon (bottom) shape examples. The Inner/Outer channels' pressure ratio is reduced from left to right, leading to a decrease in either core diameter or inner ribbon thickness. D | Fiber size reduction through the faster spinning of the multi-compartment fibers, which allows for maintenance of shape while significantly reducing the total diameter of fibers from 200 μm to less than 50 μm. E | Fiber shapes can also be maintained while incorporating distinct materials, as Gelatin Methacryloyl (GelMA) blended with GG (GelMA/GG, Orange), allowing for the manipulation of relative compartment sizes (i). The ability of GelMA to crosslink through UV light also introduces the possibility of fusing the shell of two adjacent fibers as a bottom-up strategy (ii). All scale bars are 100 μm (For interpretation of the references to color in this figure legend, the reader is referred to the web version of this article.).

gineering (TE) strategy that transports and controls the behavior of encapsulated cells. Achieving all of these structures using a single type of microfluidic chip highlights the high versatility and unprecedented application possibilities of 3D FF for the engineering and biofabrication of live-like fiber tissues and 3D models.

2. Results and discussion

2.1. Flow-Focusing yields a plethora of fiber compartment shapes

To fully assess the potential of 3D flow focusing, a custom-made microfluidic chip (**Fig. 1A, S1**) composed of four inlets and one outlet was used to flow hydrogel solutions into a Calcium Chloride ($CaCl_2$) crosslinking bath for forming hydrogel fibers upon extrusion (wet-spinning).

As model hydrogel, we used Gellan Gum (GG), an ionic-crosslinking material commonly used for tissue engineering [16], mixed with 1 µm fluorescent microparticles for tracking the final fiber shape. At room temperature, GG chains arrange into an intertwined helix conformation with the negatively charged carboxyl groups pointing outwards. Positive ions (such as Ca^{2+}) can electrically shield the carboxyl group leading to a tighter aggregation of the helices forming stable hydrogels [16,17]. The difference in viscosity between the two hydrogel/particle blends (**Fig. 1A**) was explored to understand the consequence of viscosity and flows in fiber shape and compartment organization.

By using three inlet channels of the chip and blocking the fourth, continuous fibers (**Video S1**) with the core-shell morphology (**Fig. 1B, i**) were obtained when the more viscous component was in the center channel and the less viscous one was flowing in the outer channel ($\frac{v_{inner}}{v_{outer}} > 1$), as represented by the sketches in **Fig. 1B, i**. From here, we concluded that, when flowing similar solutions within this microfluidic configuration, there is a natural preference for the more viscous component (higher resistance to deformation) to maintain its initial position on the cross-section. In contrast, the less-viscous solution tends to squeeze around the more viscous counterpart, surrounding it (**Fig. S2**). Similarly, a third material can be included in one of the center channels, yielding a tricoaxial-like shape (**Fig. 1B, iv**). Curiously, we observed that once the fourth channel was also filled with the less viscous solution, the formation of core-shell shape was no longer possible. The outer solution no longer surrounded the center one but instead pressed it, obtaining a flat, ribbon-like structure (**Fig. 1B, ii**). Similarly, the materials were alternated within the 4-channel setup, giving rise to 4 parallel compartments named double-Janus (**Fig. 1B, iii**). Using similar solutions but further modulating the

pressures within the different channel configurations yielded even more distinct and exotic shapes (**Fig. S3A)**.

To further assess continuous hydrogel FF's potential, we employed a simpler 2D FF chip where the 3D pore geometry is absent and channels meet in a T-like junction (Fig. S1). We obtained a shape that we named as double core-shell (**Fig. 1B, v**). Notably, in this more straightforward configuration where the 3D pore is absent, the different viscosities' effects seem to become less relevant. The materials flow similarly, leading to the same shape even if inner/outer viscosities are reversed (**Fig. S3, B**).

Once we observed all the possibilities of flowing hydrogel precursors in these distinct configurations, we tested the introduction of an apolar solution to form confined droplets within the outer hydrogel materials. As a model, we used mineral oil and observed the formation of a core of oil droplets within the hydrogel fiber or, in other words, the oil core-hydrogel shell structure (**Fig. 1B, vi**). Researchers have recently also demonstrated the fabrication of bubble-filled hydrogel fibers by introducing air within alginate fibers using a co-axial flow system [18]. While very interesting as a fabrication approach with possibilities for the breakage of fibers into small structures, the air is not an efficient method for transporting biologically relevant components. Instead, by introducing oil droplets in fibers, our approach facilitates the inclusion of hydrophobic features, adding a different chemical behavior to otherwise purely hydrophilic hydrogel structures.

2.2. Manipulation of fiber size and composition

Once microfiber compartment shapes were explored, we investigated how varying the applied pressures could affect flow ratios and change the relative compartment dimensions and overall microfiber sizes. During the wet-spinning process, different factors contribute to the fiber shape, among which are the applied pressure and consequent flows, the dimension of the microfluidic chip output channel, and gravitational and buoyancy forces. Overall, the microfluidic channel size will dictate the global fiber diameter ranges, which can then be slightly manipulated by controlling precursor flow through inlet pressure regulation. In all cases, the formed fiber was collected at the bottom of the coagulating bath, indicating higher gravitational forces than buoyancy forces (**Supplementary Video 1**).

From here, we observed that changing the relative inner/outer pressures and consequently flows altered the distinct compartments' size. This change led to, e.g., thick/thin core/shell or considerable changes such as for the ribbon structure (from 3 individual compartments to 2 main compartments separated by a thin sheet of a third material) (**Fig. 1C**). Furthermore, we were able to tune the flow conditions by applying pressure in a sinusoidal fashion (increasing or decreasing in time), showing that it is possible to obtain, e.g., a fiber with a constant diameter but a gradually increasing core-to-shell size ratio (**Fig. S4**).

Since the hydrogel precursors are spun into a crosslinking CaCl2 solution, it is possible to draw the fiber into the bath while crosslinking. By pulling the fiber at a higher speed than that at which it is spinning, a considerable size reduction can be achieved, leading to thinner multi-compartment hydrogel fibers. This process may influence the alignment of the hydrogel precursor's polymeric chains, which may affect the mechanical properties of the fibers. Still, drawn fibers maintain their shape even at smaller dimensions (**Fig. 1D**). With this approach, we fabricated full core-shell fibers with less than 50 μm of total diameter. This dimension represents the smallest hydrogel core-shell fiber so far fabricated, to the best of our knowledge. Most examples within the literature do not reach sizes below 200 μm [7,19]. Shao and colleagues report core-shell fibers with core dimensions approaching 75 μm, but these have a shell of around 1 mm [20]. Therefore, our approach can be highly relevant for biological applications as it is the first to approach the magnitude of single-cell size [21] and blood arterioles diameter [22]. The fact these fibers are composed of soft hydrogel compartments is also relevant as these small blood vessels, and soft biological tissues have similar mechanical properties, frequently on the 5–20 kPa stiffness range [16,23,24].

All the structures so far discussed were composed only of ionic-crosslinking GG, which is relevant for the biofabrication of different structures but limited as a single material option. As such, we investigated if other materials could be included without compromising fiber shape. We had observed that the concentration of GG and consequent viscosity could be changed and still lead to similar core-shell structures (**Fig. S5**) if the viscosity ratios were kept. With this in mind, we then blended gelatin methacryloyl (GelMA) 5% with GG 0.5% at a 1:1 ratio and still observed the formation of core-shell structures with a tunable compartment size (**Fig 1E, i)**. As the GG/GelMA blend is less viscous than the normal GG, the positive inner/outer viscosity ratio is not violated, and as described above, the requirement for core-shell shape holds. Furthermore, the possibility of GelMA to be crosslinked by UV light allowed us to imbue these fibers with two stages of crosslinking: the immediate GG ionic crosslinking upon spinning - which derives the core-shell shape - followed by the UV crosslinking of the GelMA shell component, allowing individual fibers to be fused, potentially interesting for bottom-up assembly (**Fig. 1E, ii**).

2.3. Endothelial cell-laden flow focusing core-shell

To explore the fast fabrication of core-shell structures, we approached vascular-like fibers by encapsulating endothelial cells within a soft, biolabile [24] core supported by a more robust and more stable GG shell (**Fig. 2A**). Since a pure GG core would not be remodeled by endothelial cells, a different core material is required. Several works have shown that 3D environments of 5% GelMA can naturally promote endothelial cell proliferation and tubular-like arrangements [20,25], with an inherent FF caveat: GelMA 5% solutions have very low, water-like viscosity. Even if easily mixed with GG and used to form the fiber shell (**Fig. 1D**), placing GelMA within the core flow would violate the FF viscosity ratio (inner>outer) of the core-shell shape, voiding its fabrication.

To overcome this, we blended GelMA5% in a solution of hyaluronic acid (HA) 0.5%, which allowed us to increase the viscosity of GelMA to overcome that of GG (**Fig. 2C**) and thus lead to the formation of GelMA/HA Core – GG Shell fibers (**Fig. 2B, D, S6**). Human dermal microvascular endothelial cells (hDMECs) were encapsulated within this core, remaining viable post-fabrication (**Fig. 2E, S7**). Upon cell culture, it was possible to observe the gradual migration of endothelial cells to the core/shell interface and some organization around an empty lumen, from 7 to 14 days (**Fig. 2F**). These structures were visible in some regions of the fibers on the later time points of 14 days, the frequently reported length of time to achieve such responses of endothelial tubularization [19]. However, further optimization might be required to obtain fully tubularized endothelial structures, which is the final need for a functional vascular network. We believe there is still a gap to close in finding optimal levels of cell density, material softness, and degradability to achieve continuously uniform tubularization. Researchers recently approached tubular-like channel perfusion by using cell densities one order of magnitude above the ones here tested, hinting at the importance of that parameter for efficient vascularization [26]. As a different example, the rolling of cellular layers was also recently shown to allow the fabrication of perfectly tubular endothelial structures [27]. However, these are small cellular cylinders that are still far from the vascular dimensions needed for tissue engineering applications.

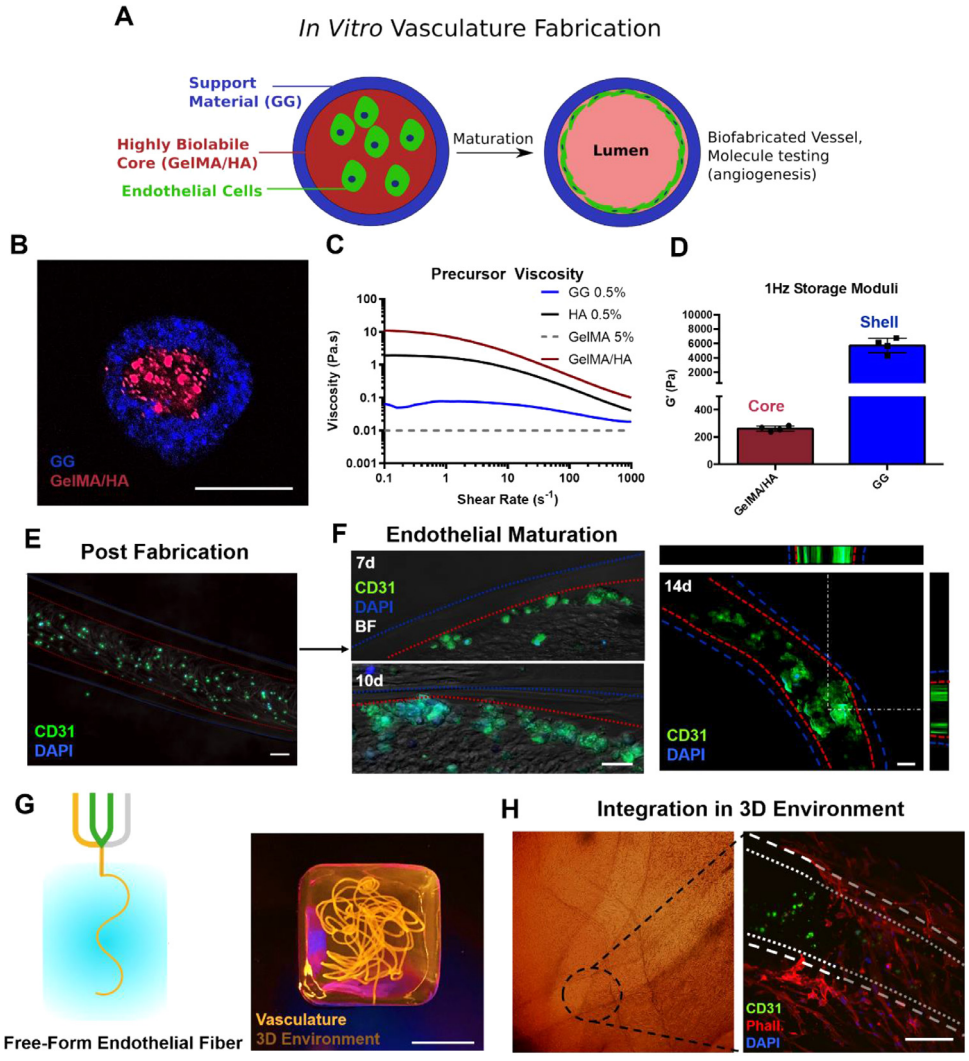

Fig. 2. Flow focusing Endothelial cell-laden Core-Shell Fibers: A | Rationale behind the core-shell structure in which the biolabile core allows endothelial cells' organization and maturation towards lumen-like tubularization. B | Core-Shell fibers with a non-ionic crosslinking, biolabile core (GelMA/HA, light red) within the GG shell (blue). Scale bar: 200 μm. C | Viscosity profiles of the different materials involved. D | Bulk mechanical characterization of both core and shell hydrogels, evidencing the full order of magnitude of difference between core and shell material's shear moduli. E | Immunocytochemistry of CD31 positive human dermal microvascular endothelial cells (hDMECs, green) within the fibers' core, post-fabrication. Scale bar: 100 μm. F | With culture time, endothelial cells are mostly present at the core/shell interface, gradually accumulating in that region. Upon 14 days of culture, certain fiber regions become more populated with endothelial cells surrounding a hollow core region, as shown on the right. Scale bars: 100 μm. G | Rationale behind the manipulation of the free-form core-shell fibers and inclusion in a 3D hydrogel environment. Scale bar: 5 mm H | Endothelial cell-laden core-shell networks within a collagen matrix populated with human dermal fibroblasts upon three days of culture (left - brightfield image, right - fluorescence image). Fibroblasts (Rhodamine-phalloidin, red) populate the collagen mesh and gradually surround the endothelial cell-laden core-shell network. Scale bar: 200 μm (For interpretation of the references to color in this figure legend, the reader is referred to the web version of this article.).

In our case, these endothelial cell-laden core-shell fibers can be spun to considerable lengths and remain free in culture. We tested the integration of fibers within a 3D environment with different cell types to explore this advantage, mimicking a natural 3D vascular network (**Fig. 2G**). The core-shell endothelial cells-laden fibers were placed within a 3D collagen matrix with encapsulated fibroblasts, co-cultured for three days, forming a complex collagen-fibroblast 3D mesh surrounding the endothelial cell-laden core-shell network (**Fig. 2H, Video S2**). The potential for fabricating considerable lengths of these vascular-like fibers and their simple integration within 3D scenarios shows explicit value in such an approach, with further focus being needed for continuous and uniform endothelial tubularization. From there, it is also essential to consider that the material in the fiber lumen must degrade towards a hollow, perfusable structure. Using GelMA/HA blends, the precursor viscosity can be increased but still result in a soft, degradable core, which can then degrade with culture time and endothelial maturation [20]. A specific flow setup can then be engineered to connect the vascular fibers to the flowing medium, which aids in removing degraded core material and its conversion to an empty, perfusable lumen.

2.4. Melanoma-on-a-ribbon shaped fiber

Once the ribbon-like fibers with two different compartments separated by a third material were observed, we explored the possibility of fabricating cancer models where one compartment could be used to encapsulate cancer cells and another to include stromal ones, separated by a basement membrane-like ribbon (**Fig. 3A**). To focus on cancer cells' behavior and potentially screen the effect of drugs within the model, we used an adhesive and degradable matrix for the cancer cell compartment and a more inert, non-biodegradable material for stromal cell encapsulation. Moreover, we hypothesized that the separating material could be one

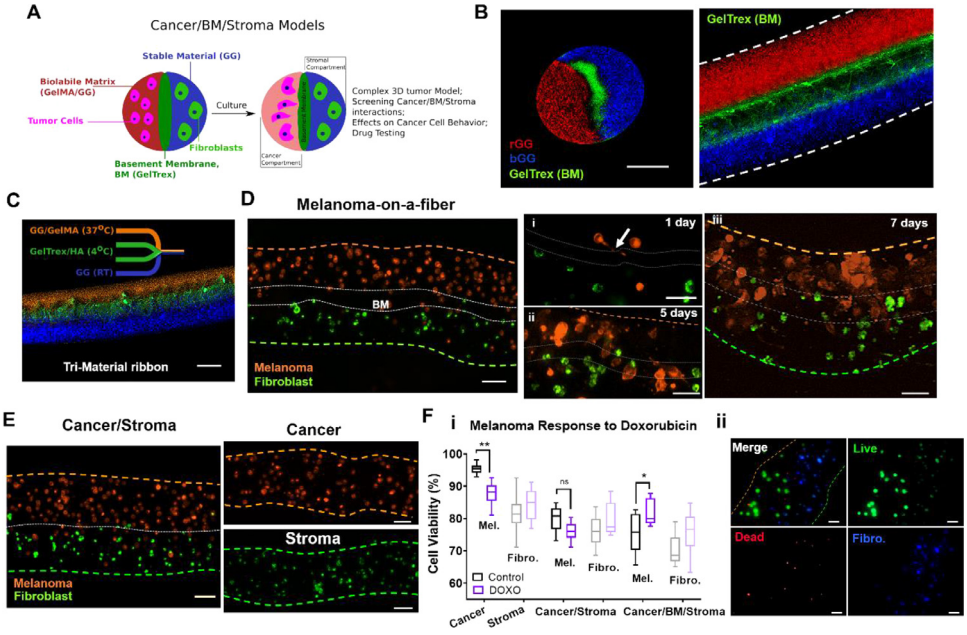

Fig. 3. Flow focusing Ribbon Cancer/BM/Stroma Fibers: A | Rationale behind the use of ribbon fibers for modeling cancer/BM/stroma in vitro. B | Inclusion of a BM-like material (GelTrex/HA, Green) in between the outer GG compartments, axial (left, fiber cut cropped into an entirely black background), and longitudinal (right) views. Scale bars: 200 μm. C | Fabrication of tri-material ribbon fibers, highlighting the material and the respective temperature used in each channel (drawing). Scale bars: 200 μm. D | Melanoma-on-a-fiber model obtained by encapsulating SK-MEL-28 cells in the cancer compartment (orange) and human dermal fibroblasts (hDFs) in the stromal compartment (green). Scale bar: 100 μm. After one day of culture, it was possible to observe melanoma cells protruding into the BM compartment (space between white-spotted lines) towards stromal cells (i, scale bar 50 μm). This behavior was even more evident after five days (ii, scale bar 50 μm) and seven days (iii), when cancer cells invaded the stroma interface. E | Modular deconstruction of fiber compartments by altering the materials/cells flowing towards simpler cancer/stroma fibers (left), stroma (bottom right), or cancer (top right). Scale bars: 100 μm. F | Proof of concept test of melanoma cell response to doxorubicin. Cell viability analysis (Calcein AM/Propidium Iodide Live/Dead) was combined with a cell tracker to detect each type's percentage of viable cells (ii). Scale bar: 50 μm. Image analysis results for the percentage of viable cancer cells (mel.) and fibroblasts (fibro.) in each model after 24 h of treatment (i). ** $p<0.01$, * $p<0.05$, ns – not significant, as derived by 2-way ANOVA followed by Sidak's multiple comparison test. No statistical significance obtained when comparing control/treatment stroma conditions (For interpretation of the references to color in this figure legend, the reader is referred to the web version of this article.).

that would mimic the native Basement Membrane (BM), which naturally bridges epithelial from stromal tissue compartments and is considered the first barrier for cancer cells entering metastasis [28]. As the recapitulation of such a scenario would be of high value for modeling cancer cell invasion and *in vitro* testing of many sorts, we first demonstrated the use of a growth-factor reduced BM analog (GelTrex) and its placement between two GG compartments following an approach similar to the one used for core-shell structures (HA blending) but with the ribbon configuration (**Fig. 3B**). From here, we increased the complexity of these structures by fabricating tri-material fibers, using a GG/GelMA 1:1 blend as the cancer compartment material, GelTrex/HA as the basement membrane, and GG alone as the stromal environment. The simplicity of our setup and fast processing times (one second inside the chip) allowed us to successfully manipulate the different materials at distinct temperatures and obtain the desired structures, with the further possibility of changing compartment size, namely BM thickness (**Fig 3C, S8A, B**).

To recapitulate cancer/BM/stroma structures, we encapsulated melanoma cells (SK-Mel-28) within the cancer compartment and human dermal fibroblasts (hDFs) within the stromal compartment, obtaining a melanoma-on-a-fiber model (**Fig. 3D**). After one day of culture, it was possible to observe melanoma cells emitting protrusions into the BM towards the stroma (**Fig. 3D, i**). This response was even more relevant upon 5 and 7 days of culture where invasive melanoma cells can be seen going through the BM compartment and reaching the stroma (**Fig. 3D, ii, iii**). The ability to change the materials that flow on-the-fly allowed Cancer/BM/Stroma fibers to simultaneously be tested with Cancer/Stroma (no BM), Stroma-only, or Cancer-only structures (**Fig. 3E**), to observe the effect of the different arrangements in the behavior of cancer cells. Even though cells are initially encapsulated within the same matrix for all cases, the number and type of fiber compartments and consequent overall cellular composition changes, and this 3D complexity affects cancer cells' response. The previously discussed cancer cell invasion was not so evident in the absence of BM and much less so when cancer cells were alone. Differences were even more apparent after seven days of culture (**Fig. S8C**). These differences in cancer cells' outcome demonstrate how important it might be to approach the biological scenario not only from a biochemical point of view but also considering the distinct materials' architecture.

It has been widely shown that basement-membrane-like proteins can widely impact cancer cell invasion and migration [29]. Further pro-invasive outcomes derive from stromal fibroblasts in the vicinity of tumor cells [30–32]. Indeed, we could observe the most significant changes in cancer cell invasion when both BM and stromal cells were present. This behavior evidences both their synergistic effects and the need for adequately approaching this complexity when attempting to, e.g., test the influence of anti-cancer drugs *in vitro*.

As a proof of concept, we tested the effects of the anti-cancer drug doxorubicin on the viability of cancer and stromal cells within these fibers with distinct architectures. Doxorubicin is a long-known drug that promotes cancer cell death by interfering with DNA replication and proliferation pathways [33]. As we could observe cancer cells responding shortly after building the model, we looked to the viability of both cell types after 24 h of culture. To do so, we combined a live/dead assay with fluorescent tracking of fibroblasts to quantify and derive the number of viable cells of each type after treatment (**Fig. 3F**). Curiously, after treatment with doxorubicin, different responses could be observed depend-

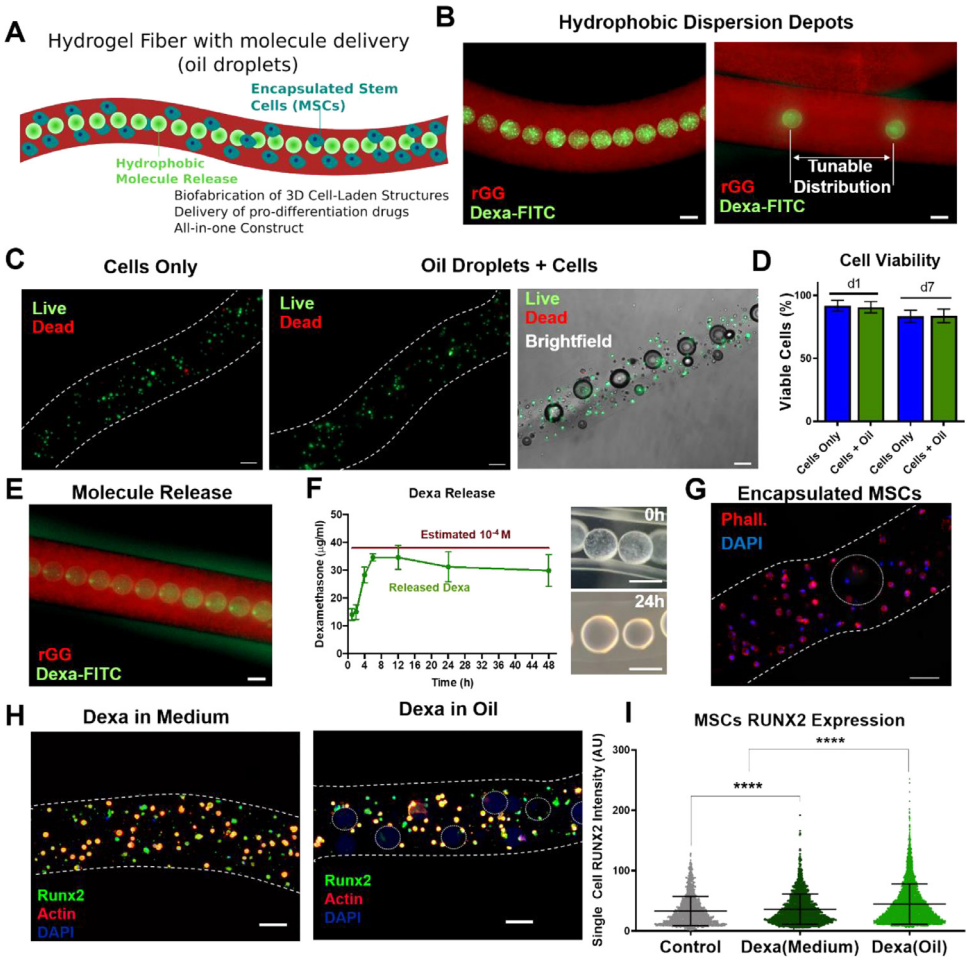

Fig. 4. Multi-Chemistry Biofabrication: A | Rationale behind the fabrication of hydrogel fibers of a biolabile GG/GelMA matrix (red) with oil droplets containing hydrophobic molecules (green) to stimulate encapsulated stem cells (blue). B | Fluorescent imaging of the fibers with sesame oil droplets containing Dexamethasone-FITC (Dexa-FITC). C | Assessment of BMMSC viability in the fibers with (cells + oil) and without (cells only) oil droplets. Scale bars: 100 μm D| Similar viability upon live/dead quantification after one day and up to 1 week of culture. E | Release of Dexa-FITC from the fibers when these are kept in PBS (right). Scale bar: 100 μm. F | Quantification of the Dexamethasone released from fibers incubated in PBS as measured (green curve) compared to the theoretical estimation of concentration upon full release (red line represents the maximum estimated concentration). On the right, brightfield images of the oil droplets within the fibers after fabrication (0 h) and upon 24 h of incubation. Scale bar: 50 μm. G | Encapsulated BMMSC morphology in the vicinity of an oil droplet. H | Representative immunocytochemistry images of hydrogel fibers (limited by dashed white lines) encapsulating BMSCs stained for Runx2 (Green), Actin (Red), and DNA (blue) after culture in the presence of Dexamethasone provided in the medium or released from the oil droplets (highlighted with white circles) Scale bars: 100 μm. G | quantification of single-cell Runx2 signal intensity. Cells in the fibers are cultured in standard culture medium (control), the same supplemented with 10^{-6} M soluble dexamethasone (Dexa in Medium) or in the fibers with oil droplets containing dexamethasone (Dexa in Oil). **** $p<0.0001$ as derived from One-way ANOVA followed by Kruskal-Wallis multi-comparison test (For interpretation of the references to color in this figure legend, the reader is referred to the web version of this article.).

ing on the model's complexity. Stromal cells, encapsulated in a mostly inert matrix, did not suffer any significant change in viability. Cancer cells, on the other hand, responded to the drug. As one could expect, a significant decrease in cancer cell viability was seen on cancer-only fibers, but this response changed as the complexity of the 3D model increased. With the presence of fibroblasts, the decrease in cancer cell viability was no longer significant. Oppositely to cancer-only fibers, in the more complex model composed of stromal cells and a BM, the viability of melanoma cells treated with doxorubicin was higher than those of non-treated cells (**Fig. 3F, S9**). As it seems, the presence of fibroblasts exerts a protective effect on the doxorubicin-induced cancer cell death, a response that has been previously observed in organotypic models of the disease [34]. Partly, this might be due to fibroblast-melanoma cell communication, which can stimulate cancer cells' pro-survival mechanisms to overcome the drug's effect [35,36].

Furthermore, additional mechanisms to overcome doxorubicin-induced cancer cell death appear to be at play once a BM-like matrix separates cancer and stroma. Even though this particular response type was not reported previously, it is well described that doxorubicin's effects are intimately related to cell motility and adhesion [37]. This drug's impact might be diminished when cancer cells can migrate through the extracellular matrix (ECM)-like gels versus standard culture conditions [38]. As such, we believe that the pro-survival stimulation by fibroblasts nullifies the negative effect of the doxorubicin treatment on cancer cells. When this is combined with a highly biolabile BM-like matrix, melanoma cells can further move and proliferate with ease and effectively recover from the doxorubicin challenge. Indeed, the effects we could observe warrant further investigation on this particular response.

Nevertheless, this test demonstrates that our novel melanoma-on-a-fiber platform can integrate several of the previously reported intricacies on cancer cell responses to doxorubicin due to the novel combination of 3D environments, multi-compartment, multi-material, and multi-cellular architectures. It also highlights how significant it might be to recapitulate the complexity of live tissues to derive the most relevant responses, as oversimplification can lead to different and eventually erroneous conclusions.

2.5. All-in-one multi-chemistry tissue engineering

As a more distinct structure, we explored the biological potential of the hydrogel fibers with an oil droplet core. The introduction of apolar solutions opens the possibility of transporting hydrophobic molecules within a highly hydrophilic hydrogel structure. The distinct polar/apolar compartments, therefore, represent a unique platform to transport cells in a 3D construct (polar hydrogel) together with pro-differentiation hydrophobic molecules within isolated depots (apolar droplets) (**Fig. 4A**).

We initially verified that distinct pressure/flow ratios between the hydrogel sheath and the oil core allowed the fabrication of structures with oil droplets of different sizes and distribution, where hydrophobic dexamethasone could be dispersed (**Fig. 4B, S10**). Knowing these structures were possible, our priority was to confirm if cells could be encapsulated within these fibers with oil droplets without any adverse impact on viability. Indeed, we demonstrated that the introduction of oil had no adverse effect on the viability of Bone Marrow Mesenchymal Stromal Cells (BMMSCs) for up to 7 days in culture (**Fig. 4C, D**) nor on the morphology of these cells (**Fig. 4G**), regardless of their proximity to the oil droplets. Overall, cells behaved similarly to those in hydrogel fibers without oil.

After this initial validation, we tested the hypothesis that the oil compartment could be used to transport hydrophobic molecules that could direct the differentiation of BMMSCs, replacing the use of soluble factors in the medium in an all-in-one approach (**Fig. 4A**). Dexamethasone is a synthetic corticosteroid used in stem cell differentiation protocols, frequently modified to become water-soluble and used in the cell culture medium. Alternatively, using the oil core, we could transport the unmodified molecule, observing its gradual release into the medium (**Fig. 4E, F, S11**). Dexamethasone was previously shown to directly impact BMMSC osteogenic differentiation by promoting Runx2 expression [39]. We compared the effect of transporting and releasing pure dexamethasone from the oil droplets in BMMSCs encapsulated in 3D GG:GelMA fibers with the impact of the drug present in the culture medium (**Fig. 4H, S12**). Based on the expression of Runx2, we demonstrate that the dexamethasone released from the oil could not just replace soluble dexamethasone but stimulate cells even more potently (**Fig. 4I**). This difference can be a consequence of two different events. First, by transporting the unmodified dexamethasone molecule, we might be looking at a different extent of cell-drug interaction than the water-soluble Dexamethasone counterpart, which is long-known to happen within organisms [40]. Second, having a gradual (within hours) release, instead of a single burst, more closely mimics the way corticosteroids are produced and see their concentrations fluctuate within the organism [41], which might also have an impact on the consequent cell responses.

Even though we have employed a simple dispersion in oil, there are more possibilities to explore in the future to tune dexamethasone release, such as binding it directly to the oil [42] or even transporting it within liposomes [43]. Using strategies such as this one may be relevant for distinct tissue engineering approaches where both stem cells and the hydrophobic molecules that drive their differentiation can be integrated within the same structure. As demonstrated, the transport of unmodified hydrophobic molecules might potentially lead to improved differentiation outcomes. Simultaneously, these molecules are not added to the culture but transported within the same 3D construct, which might facilitate its application as an all-in-one tissue engineering approach.

3. Conclusions

We have employed a hydrodynamic 3D flow-focusing setup to fabricate hydrogel fibers with various multi-compartment shapes and organizations. Using a single chip, we show how manipulating pressure and tuning material's viscosity and different channel organizations can be employed to fabricate very different fibers, from hydrogels and hydrophobic core-shell to ribbon-like structures. We further explore how the pressure and consequent flow can manipulate the separate compartments' size and how these fibers can be drawn immediately after crosslinking, maintaining the same compartments' shapes and resulting in full diameters below 50 µm.

To prove the potential of our strategy for the biofabrication of diverse structures, we started by showing how flow-focusing can match existing systems and recapitulate structures such as the core-shell fibers. In these fibers, endothelial cells can be introduced and gradually organize overtime. Also, by forming free-floating fibers, our approach allowed us to easily incorporate these fibers within a 3D environment created by distinct materials and cell types, quickly obtaining a vascular-like network that can be cultured inside other engineered tissues.

High novelty is also presented by the fabrication of melanoma-on-a-fiber models using a triple ribbon shape to recreate Cancer/Basement Membrane/Stroma tissue organization. Within these fibers, cancer cells' invasive behavior can be recapitulated, and detailed responses to anti-cancer drugs can be analyzed instead of traditional models that are limited in representing the complexity of living tissues.

Finally, we show how hydrophobic fluids can be combined with the hydrogels by integrating a core of oil droplets within a hydrogel fiber encapsulating BMMSCs. By dispersing pure dexamethasone within the oil, we show that its release can promote the expression of Runx2 (osteogenic regulator and early marker) by the cells to a greater extent than that of soluble dexamethasone dissolved in the culture medium. This strategy represents an all-in-one tissue engineering and molecule delivering approach.

Overall, we demonstrate the potential of 3D FF to fabricate hydrogel structures with various shapes, compartments, materials, and cells. These, in turn, can be used to engineer biological-like tissues for regeneration or for creating 3D models with high biological relevance for a wide variety of *in vitro* tests, such as vascularization responses or cancer drug testing. This broadly adaptable fabrication was possible by manipulating materials and flows with the same technique and setup, using a single microfluidic chip.

4. Materials and methods

4.1. General flow focusing fabrication of multi-shape fibers

Gellan Gum (Gelzan, Sigma) was used as the ionic gelling material for all the reported hydrogel fiber shapes. GG (Gellan Gum) was dissolved at 0.5 wt.% in water containing 0.25 M sucrose as previously described [44]. GG was blended with red or blue, fluorescent microparticles (screenMag, Chemicell), 1:10 particle dilution for color tracking distinct compartments.

Fibers were fabricated using one single chip geometry (3D Flow Focusing, Dolomite) (Fig. S1). The Double Core-Shell Shape was the only structure fabricated with a different chip (2D Flow Focusing, Dolomite). The chips were connected to a digitally controlled microfluidic pump system (OB1, Elveflow), which directly applied pressure to individual Eppendorf's containing the distinct materials, connected to the chip by 30 cm of polytetrafluoroethylene microfluidic tubing (0.5 × 1.6 mm). The fibers were formed upon crosslinking (wet spinning) in a 0.1 M $CaCl_2$ bath.

Slight variations on the setup led to the distinct fiber shapes. Flowing red-labelled GG in the 2 inside channels and blue-labelled GG in the 2 outer ones formed hydrogel fibers with a ribbon-like shape (3 compartments). Core-Shell fibers were produced by blocking the flow of one of the outer channels, allowing the inner flow to be surrounded by the outer one.

The oil-core hydrogel-shell was formed by flowing an apolar solution in the inner channels and GG in the outer ones. The tricoaxial shape was produced by flowing 2 distinct materials (GG and red-GG) in the inner channels in the core-shell configuration.

Double-Janus fibers were fabricated by alternating the materials flowing in the ribbon configuration, leading to the 4 distinct compartments (red-blue-red-blue or blue-red-blue-red).

The double core-shell shape was produced taking advantage of a Flow Focusing chip, without the 3D pore geometry, which allows the inner material to go around and surround the outer ones forming 2 compartments separated and covered by a third one.

4.2. Size and composition manipulation

The inlet pressures were tuned to manipulate the relative sizes of the core-shell and ribbon-shaped compartments, and these were directly responsible for larger/smaller compartments upon flowing with higher/lower pressures. In order to reduce the global fiber diameter, these were pulled immediately after spinning in the $CaCl_2$ bath, with gradually increased speeds leading to gradually smaller diameters.

To prove that shapes could still be obtained by the combination of different materials, a blend of 1:1 GG 0.5%:GelMA5% was used as a shell solution. These fibers were collected upon spinning in the bath and further crosslinked under UV light (320–500 nm) (Omnicure series 2000) for 50 s at 0.6 mW/cm2. Fibers were also fused by crosslinking the shells when in close contact.

4.3. Core-Shell, endothelial cell-laden fibers

In order to increase GelMA viscosity above that of GG to create the core-shell fibers with a biolabile core, GelMA was dissolved in a solution of Hyaluronic Acid (Sodium Hyaluronate 1.5MDa, Lifecore) containing 0.25 M sucrose and 0.3% Irgacure (Sigma). Differences in viscosity were studied using a Malvern Kinexus Pro+ Rheometer and a cone plate geometry (40 mm/ 4°), where the shear viscosity was recorded along a range of 0.1–1000s^{-1} of Shear Rate. Oscillation tests were also performed to characterize the mechanical properties (Shear Modulus) of GG (shell) and GelMA/HA (core) hydrogels. Briefly, an amplitude sweep at 1 Hz was performed to derive the linear viscoelastic region, within which a frequency sweep was then performed to derive the storage (G') and loss (G") shear moduli of the hydrogels.

To produce vascular structures, human dermal microvascular endothelial cells (hDMECs) were suspended in the core solution of GelMA/HA prior to the fiber fabrication at a density of 3E6 cells/mL. Fibers were spun into the $CaCl_2$ solution and afterwards exposed to UV light (as previously reported) to crosslink the GelMA/HA core. To obtain fibers with a liquified core, the UV crosslinking step was skipped.

Post-fabrication endothelial cell viability was assessed by incubation with medium containing 1:1000 dilution of Calcein AM (Thermofisher) and 1 μg/mL Propidium Iodide (Molecular Probes) for 30 mins at 37 °C, 5% CO_2 and cells were then imaged under a fluorescent Axio Observer Inverted Microscope (Zeiss).

For CD31 immunocytochemistry, fibers were fixed in formalin 10% for 10 mins at room temperature (RT), washed with PBS and incubated with 0.2% Triton X-100 (Thermo Fisher) in PBS for 12 min to enhance cell membrane permeability. After washing, non-specific interactions were blocked by incubating with 3% BSA (Sigma) in PBS for 30 min. Afterward, samples were incubated with the primary mouse CD31 antibody (DAKO, 1:50 dilution) in 1% BSA overnight at 4 °C. These were then incubated with the secondary anti-mouse antibody (Alexa 488 donkey anti-mouse, Invitrogen, 1:500 dilution) for 1 h at RT. At this stage, cell cytoskeleton and nuclei were also stained by adding Phalloidin-TRITC (Sigma) at 2ug/mL and DAPI (Biotium) at 4ug/mL. Afterwards, samples were taken to image in the fluorescent microscope.

To integrate vascular core-shell fibers in the 3D environments, human dermal fibroblasts (hDFs) were suspended at a density of 3E6/mL in a 2 mg/mL solution of neutralized rat tail collagen type I (Gibco). Core-Shell endothelial cell-laden fibers were randomly placed within well plates and the fibroblast-containing collagen solution was added to these and crosslinked by incubating at 37 °C. After 3 days of culture, samples were fixed and stained as previously described. To obtain 3D rendition of the environments, samples were imaged with a Z1 Light Sheet Microscope (Zeiss). Throughout this experiment, Fibroblasts were cultured in complete alpha-MEM medium (Gibco), hDMECs were cultured in EGM-2 Bullet medium (Lonza) and co-cultures were kept with 1:1 mix of both media.

4.4. Ribbon shaped, cancer/BM/stroma fibers

To obtain the BM structure within the 2 compartments, an overnight-thawed GelTrex Solution (Gibco) was mixed with the previously described Hyaluronic Acid 0.5% solution in order to yield a final GelTrex concentration of at least 9 mg/mL according to the manufacturer's requirements for the formation of a gel. To observe GelTrex within the outer Gellan Gum compartments, the Blue and Red particles in the GG were used and GelTrex was mixed with a 1:100 dilution of a 1% GG-FITC solution. For obtaining the tri-material FF, a similar approach was followed, but instead of having GG 0.5% on both sides, one was replaced by GG/GelMA 1:1 blend. The distinct materials were kept at different temperatures during fabrication by maintaining the respective reservoir at RT (GG), 37 °C (GelMA), and 4 °C (GelTrex/HA) to ensure fluidity within the chip. Fibers were collected in the $CaCl_2$ bath, then the GelMA component was crosslinked by quick UV exposure (as previously described) and the GelTrex/HA was crosslinked by placing fibers in incubation at 37 °C. Melanoma cells of the Sk-MEL-28 (ATCC) cell line were encapsulated in the GG/GelMa compartment, and fibroblasts (hDFs) were encapsulated in the GG compartment, both representing cancer and stroma, respectively, separated the GelTrex/HA. To track the different cell types, these were stained with CellBrite Green and Orange (Biotium) according to the manufacturer's instructions.

To fabricate the different modular fibers, we opened and/or blocked specific inlets, from flowing all (Cancer/BM/Stroma) to only the side channels (Cancer/Stroma, no BM) or individual ones (Stroma- and Cancer-alone). Fibers with tracked cells were observed under an Inverted Confocal Laser Scanning Microscope (Leica), throughout 1 week of culture.

For the drug tests, fibroblasts were stained prior to encapsulation using the CellTracker blue CMAC Dye (Molecular Probes) according to the manufacturer's instructions. These were then integrated into the fibers together with the cancer cells. 24 h after fabrication, fibers were incubated with either culture medium (no treatment) or culture medium containing 1 μM of Doxorubicin (Carbosynth). 1 day after treatment, samples were incubated with Calcein AM/PI as previously described for viability assessment. Images of the fibers were acquired in the fluorescent microscope and a cell profiler [45] pipeline was used to derive the numbers of live and dead cells using the blue staining to distinguish fibroblasts from melanoma cells.

Throughout the experiment, fibroblasts were cultured in complete alpha-MEM medium, melanoma cells in EMEM medium (ATCC) and co-cultures with a 1:1 mix of both media.

4.5. Oil-Core hydrogel-shell fibers

Fibers of GG/GelMA 1:1 encapsulating MSCs alone or including oil droplets were fabricated by wet spinning as previously de-

scribed. After 1 day and 1 week of culture in alpha-MEM complete medium, the viability of cells was assessed through the previously detailed incubation with Calcein/PI, imaging and cell counting. The morphology of encapsulated cells was observed by fixing fibers and incubating with Phalloidin-TRITC (Sigma) 2 μg/mL and DAPI (Biotium) 4 μg/mL for 1 h at RT.

To visualize fibers with oil droplets containing dexamethasone, the labelled Dexamethasone-FITC (Molecular Probes) was dispersed in sesame oil by stirring at a concentration of 0.25 mg/mL. When a uniform dispersion was obtained, fibers were fabricated and imaged under the fluorescent microscope.

To quantify the release of dexamethasone from the oil droplets, a Dexamethasone standard curve was obtained using solutions of pure Dexamethasone (Sigma) and its characteristic absorbance at 241 nm. Using this information, dexamethasone was dispersed in mineral oil at a concentration of 20 mg/mL, estimated to yield a final concentration in 1 mL of PBS of 10^{-4} M (estimated, upon total release from the oil as detailed in **Fig. S11**), high enough to be able to detect its gradual increase in concentration, measured through the 241 nm absorbance on a microplate reader (SYNERGY, Bio-tek instruments). The release was measured by keeping fibers in 6-well plates with 1 mL of PBS, and removing 100μL of the well solution for measuring, replacing by 100μL of fresh PBS for up to 48 h. Brightfield images of the oil droplets were also acquired to observe the presence/absence of dispersed dexamethasone.

To evaluate the effect of dexamethasone in oil within the 3D fibers, MSCs were encapsulated in 1:1 GG:GelMA fibers and cultured in standard medium, medium with 10^{-6} M of water-soluble dexamethasone (dexa in medium) or combined with oil droplets containing a dispersion of 0.5 mg/mL Dexamethasone (estimated to release up to the same 10^{-6} M). After 72 h in culture, fibers with the cells were fixed and immunostained against Runx2 (Mouse Anti-Runx2 (Millipore), 1:300 dilution) and later incubated with Alexa 488 donkey-anti-mouse secondary antibody (1:500 dilution, Invitrogen) as well as with Phalloidin-TRITC (Sigma) 2 μg/mL and DAPI (Biotium) 4 μg/mL. These were then imaged in the fluorescent Axio Observer Inverted Microscope (Zeiss) to observe the expression of Runx2 and Cell Profiler was used to quantify the intensity of all Runx2+ cell events. Thousands of single cells were analyzed per condition. Details of the different conditions were also imaged using the Inverted Confocal Laser Scanning Microscope (Leica).

Data availability

All data from this paper is available upon reasonable request to corresponding author.

Declaration of Competing Interest

The authors declare that they have no known competing financial interests or personal relationships that could have appeared to influence the work reported in this paper.

CRediT authorship contribution statement

Carlos F. Guimarães: Conceptualization, Methodology, Validation, Formal analysis, Investigation, Writing – original draft. **Luca Gasperini:** Methodology, Validation, Investigation, Writing – review & editing. **Alexandra P. Marques:** Conceptualization, Resources, Writing – review & editing, Supervision. **Rui L. Reis:** Supervision, Resources, Project administration, Funding acquisition, Writing – review & editing.

Acknowledgements

The authors acknowledge financial support from the European Research Council, grant ERC-2012-ADG 20120216-321266 (project ComplexiTE). C. F. G. acknowledges scholarship PD/BD/135253/2017 from Fundação para a Ciência e Tecnologia (FCT).

Supplementary materials

Supplementary material associated with this article can be found, in the online version, at doi:10.1016/j.apmt.2021.101013.

References

[1] H. Onoe, T. Okitsu, A. Itou, M. Kato-Negishi, R. Gojo, D. Kiriya, K. Sato, S. Miura, S. Iwanaga, K. Kuribayashi-Shigetomi, Y.T. Matsunaga, Y. Shimoyama, S. Takeuchi, Metre-long cell-laden microfibres exhibit tissue morphologies and functions., Nat. Mater. 12 (2013) 584.
[2] E. Kang, G.S. Jeong, Y.Y. Choi, K.H. Lee, A. Khademhosseini, S.H. Lee, Digitally tunable physicochemical coding of material composition and topography in continuous microfibres., Nat. Mater. 10 (2011) 877.
[3] S.J. Shin, J.Y. Park, J.Y. Lee, H. Park, Y.D. Park, K.B. Lee, C.M. Whang, S.H. Lee, "On the fly" continuous generation of alginate fibers using a microfluidic device., Langmuir 23 (2007) 9104.
[4] X. Du, Q. Li, G. Wu, S. Chen, Multifunctional Micro/Nanoscale Fibers Based on Microfluidic Spinning Technology., Adv. Mater. (2019) 1903733.
[5] Y. Jun, E. Kang, S. Chae, S.H. Lee, Microfluidic spinning of micro- and nano-scale fibers for tissue engineering., Lab Chip 14 (2014) 2145.
[6] L. Leng, A. McAllister, B. Zhang, M. Radisic, A. Günther, Mosaic hydrogels: One-step formation of multiscale soft materials., Adv. Mater. 24 (2012) 3650.
[7] M. Kato-Negishi, H. Onoe, A. Ito, S. Takeuchi, Rod-Shaped Neural Units for Aligned 3D Neural Network Connection., Adv. Healthc. Mater. 6 (2017) 1.
[8] J.M. Grolman, D. Zhang, A.M. Smith, J.S. Moore, K.A. Kilian, Rapid 3D Extrusion of Synthetic Tumor Microenvironments., Adv. Mater. 27 (2015) 5512.
[9] Y. Cheng, F. Zheng, J. Lu, L. Shang, Z. Xie, Y. Zhao, Y. Chen, Z. Gu, Bioinspired multicompartmental microfibers from microfluidics., Adv. Mater. 26 (2014) 5184.
[10] P. Xu, R. Xie, Y. Liu, G. Luo, M. Ding, Q. Liang, Bioinspired Microfibers with Embedded Perfusable Helical Channels., Adv. Mater. 29 (2017) 1.
[11] Y. Cheng, Y. Yu, F. Fu, J. Wang, L. Shang, Z. Gu, Y. Zhao, Controlled Fabrication of Bioactive Microfibers for Creating Tissue Constructs Using Microfluidic Techniques., ACS Appl. Mater. Interfaces 8 (2016) 1080.
[12] S. Takeuchi, P. Garstecki, D.B. Weibel, G.M. Whitesides, An axisymmetric flow–focusing microfluidic device., Adv. Mater. 17 (2005) 1067.
[13] Y.J. Chiu, S.H. Cho, Z. Mei, V. Lien, T.F. Wu, Y.H. Lo, Universally applicable three--dimensional hydrodynamic microfluidic flow focusing., Lab Chip 13 (2013) 1803.
[14] M. Rhee, P.M. Valencia, M.I. Rodriguez, R. Langer, O.C. Farokhzad, R. Karnik, Synthesis of size-tunable polymeric nanoparticles enabled by 3D hydrodynamic flow focusing in single-layer microchannels., Adv. Mater. 23 (2011) 79.
[15] J. Carneiro, J.B.L.M. Campos, J.M. Miranda, High viscosity polymeric fluid droplet formation in a flow focusing microfluidic device – Experimental and numerical study., Chem. Eng. Sci. 195 (2019) 442.
[16] C.F. Guimarães, L. Gasperini, R.S. Ribeiro, A.F. Carvalho, A.P. Marques, R.L. Reis, High-throughput fabrication of cell-laden 3D biomaterial gradients., Mater. Horiz. 7 (2020) 2414.
[17] L. Gasperini, J.F. Mano, R.L. Reis, Natural polymers for the microencapsulation of cells., J. R. Soc. Interface 11 (2014) 20140817.
[18] A.S. Chaurasia, S. Sajjadi, Transformable bubble-filled alginate microfibers via vertical microfluidics., Lab Chip 19 (2019) 851.
[19] Q. Pi, S. Maharjan, X. Yan, X. Liu, B. Singh, A.M. van Genderen, F. Robledo–Padilla, R. Parra-Saldivar, N. Hu, W. Jia, C. Xu, J. Kang, S. Hassan, H. Cheng, X. Hou, A. Khademhosseini, Y.S. Zhang, Digitally Tunable Microfluidic Bioprinting of Multilayered Cannular Tissues., Adv. Mater. (2018) 1706913.
[20] L. Shao, Q. Gao, H. Zhao, C. Xie, J. Fu, Z. Liu, M. Xiang, Y. He, Mini Tissue with Morphology-Controllable GelMA Microfibers., Small 14 (2018) 1.
[21] G.T. Charras, M.A. Horton, Single cell mechanotransduction and its modulation analyzed by atomic force microscope indentation., Biophys. J. 82 (2002) 2970.
[22] C.M. Peppiatt, C. Howarth, P. Mobbs, D. Attwell, Bidirectional control of CNS capillary diameter by pericytes., Nature 443 (2006) 700.
[23] J. Muller-Delp, S.A. Spier, M.W. Ramsey, L.A. Lesniewski, A. Papadopoulos, J.D. Humphrey, M.D. Delp, Effects of aging on vasoconstrictor and mechanical properties of rat skeletal muscle arterioles., Am. J. Physiol. - Hear. Circ. Physiol. 282 (2002) 1843.
[24] C.F. Guimarães, L. Gasperini, A.P. Marques, R.L. Reis, The stiffness of living tissues and its implications for tissue engineering., Nat. Rev. Mater. 5 (2020) 351.
[25] J.W. Nichol, S.T. Koshy, H. Bae, C.M. Hwang, S. Yamanlar, A. Khademhosseini, Cell-laden microengineered gelatin methacrylate hydrogels., Biomaterials 31 (2010) 5536.
[26] S. Maharjan, C. Ca, S. Maharjan, J. Alva, C. Ca, G. Rubio, D. Herna, Article Symbiotic Photosynthetic Oxygenation within 3D-Bioprinted Vascularized Tissues Symbiotic Photosynthetic Oxygenation within 3D-Bioprinted Vascularized Tissues., Matter (2020) 1.

[27] Q. Jin, A. Bhatta, J.V. Pagaduan, X. Chen, H. West-Foyle, J. Liu, A. Hou, D. Berkowitz, S.C. Kuo, F.B. Askin, T.D. Nguyen, D.H. Gracias, L.H. Romer, Biomimetic human small muscular pulmonary arteries., Sci. Adv. 6 (2020), doi:10.1126/sciadv.aaz2598.
[28] D.R. Sherwood, Cell invasion through basement membranes: an anchor of understanding., Trends Cell Biol. 16 (2006) 250.
[29] G. Benton, H.K. Kleinman, J. George, I. Arnaoutova, Multiple uses of basement membrane-like matrix (BME/Matrigel) in vitro and in vivo with cancer cells., Int. J. Cancer 128 (2011) 1751.
[30] B. Erdogan, M. Ao, L.M. White, A.L. Means, B.M. Brewer, L. Yang, M.K. Washington, C. Shi, O.E. Franco, A.M. Weaver, S.W. Hayward, D. Li, D.J. Webb, Cancer-associated fibroblasts promote directional cancer cell migration by aligning fibronectin., J. Cell Biol. 216 (2017) 3799.
[31] V. Luga, L. Zhang, A.M. Viloria-Petit, A.A. Ogunjimi, M.R. Inanlou, E. Chiu, M. Buchanan, A.N. Hosein, M. Basik, J.L. Wrana, Exosomes mediate stromal mobilization of autocrine Wnt-PCP signaling in breast cancer cell migration., Cell 151 (2012) 1542.
[32] A. Glentis, P. Oertle, P. Mariani, A. Chikina, F. El Marjou, Y. Attieh, F. Zaccarini, M. Lae, D. Loew, F. Dingli, P. Sirven, M. Schoumacher, B.G. Gurchenkov, M. Plodinec, D.M. Vignjevic, Cancer-associated fibroblasts induce metalloprotease-independent cancer cell invasion of the basement membrane., Nat. Commun. 8 (2017) 1.
[33] C.F. Thorn, C. Oshiro, S. Marsh, T. Hernandez-Boussard, H. McLeod, T.E. Klein, R.B. Altman, Doxorubicin pathways: pharmacodynamics and adverse effects., Pharmacogenet. Genomics 21 (2011) 440.
[34] M. Tiago, E.M. De Oliveira, C.A. Brohem, P.C. Pennacchi, R.D. Paes, R.B. Haga, A. Campa, S.B. De Moraes Barros, K.S. Smalley, S.S. Maria-Engler, Fibroblasts protect melanoma cells from the cytotoxic effects of doxorubicin., Tissue Eng. - Part A 20 (2014) 2412.
[35] E.H. Flach, V.W. Rebecca, M. Herlyn, K.S.M. Smalley, A.R.A. Anderson, Fibroblasts contribute to melanoma tumor growth and drug resistance., Mol. Pharm. 8 (2011) 2039.
[36] G. Li, K. Satyamoorthy, F. Meier, C. Berking, T. Bogenrieder, M. Herlyn, Function and regulation of melanoma-stromal fibroblast interactions: When seeds meet soil., Oncogene 22 (2003) 3162.
[37] L.A. Repesh, S.R. Drake, M.C. Warner, S.W. Downing, R. Jyring, E.A. Seftor, M.J.C. Hendrix, J.B. McCarthy, driamycin-induced inhibition of melanoma cell invasion is correlated with decreases in tumor cell motility and increases in focal contact formation., Clin. Exp. Metastas. 11 (1993) 91.
[38] R. Harisi, J. Dudás, F. Tímár, G. Pogány, S. Paku, J. Tímár, I. Kovalszky, M. Szendroi, A. Jeney, Antiproliferative and antimigratory effects of doxorubicin in human osteosarcoma cells exposed to extracellular matrix., Anticancer Res. 25 (2005) 805.
[39] F. Langenbach, J. Handschel, Effects of dexamethasone, ascorbic acid and β-glycerophosphate on the osteogenic differentiation of stem cells in vitro., Stem Cell Res. Ther. 4 (2013) 1.
[40] T. Siegal, T. Siegal, E. Shohami, Y. Shapira, Comparison of soluble dexamethasone sodium phosphate with free dexamethasone and indomethacin in treatment of experimental neoplastic spinal cord compression., Spine (Phila. Pa. 1976) 13 (1988) 1171.
[41] B.P. Schimmer, J.W. Funder, ACTH, Adrenal Steroids, and Pharmacology of the Adrenal Cortex., Goodman Gilman's Pharmacol. Basis Ther. 12e (2011).
[42] Z. Liu, L. Cao, C. Bao, S. Dong, K. Dai, L. Zhu, Cross-linked vegetable oil with covalently loaded dexamethasone: Linear drug release for osteogenic induction of hBMSCs in vitro., Soft Matter 9 (2013) 5609.
[43] N. Monteiro, A. Martins, D. Ribeiro, S. Faria, N.A. Fonseca, J.N. Moreira, R.L. Reis, N.M. Neves, On the use of dexamethasone-loaded liposomes to induce the osteogenic differentiation of human mesenchymal stem cells., J. Tissue Eng. Regen. Med. (2015), doi:10.1002/term.1817.
[44] A.F. Carvalho, L. Gasperini, R.S. Ribeiro, A.P. Marques, R.l. Reis, Control of osmotic pressure to improve cell viability in cell-laden tissue engineering constructs., J. Tissue Eng. Regen. Med. 12 (2018) e1063.
[45] L. Kamentsky, T.R. Jones, A. Fraser, M.A. Bray, D.J. Logan, K.L. Madden, V. Ljosa, C. Rueden, K.W. Eliceiri, A.E. Carpenter, Improved structure, function and compatibility for cellprofiler: Modular high-throughput image analysis software., Bioinformatics 27 (2011) 1179.